Available online at www.sciencedirect.com
ScienceDirect
International Journal of Heat and Mass Transfer 50 (2007) 782–788
International Journal of HEAT and MASS TRANSFER
www.elsevier.com/locate/ijhmt

Limitations of the standard Bernoulli equation method for evaluating Pitot/impact tube data

S.K.S. Boetcher *, E.M. Sparrow

Laboratory for Heat Transfer Practice, Department of Mechanical Engineering, University of Minnesota, Minneapolis, MN 55455-0111, USA

Received 21 July 2005; received in revised form 20 January 2006
Available online 16 November 2006

Abstract

The inaccuracies of Pitot or impact tubes for the measurement of low fluid velocities have been demonstrated by several experimental investigations. However, owing to considerable data scatter, there does not exist a definitive criterion for establishing when these instruments are inaccurate with respect to low velocities. It is not that the instruments themselves are faulty, but rather that the methodology for extracting velocity information from the measured pressures fails. The standard method for extracting velocities from the pressure data is the application of Bernoulli's equation. That equation is, however, based on an inviscid model. At low Reynolds numbers, the viscosity exerts a strong effect on the flow pattern and, thereby, invalidates the use of the Bernoulli equation. In the present investigation, a painstaking numerical simulation has been performed to establish criteria at which the Bernoulli interpretation of Pitot/impact tube data is not valid. Two types of nose pieces for Pitot/impact tube were investigated. One of these is a hemispherical nose, while the other is a flat-faced nose. It was found that for the former, the Bernoulli interpretation should not be used when $\rho U_\infty R_{\mathrm{outer}}/\mu < 45$, while for the latter, the corresponding criterion is $\rho U_\infty R_{\mathrm{outer}}/\mu < 65$. These values correspond to a 2% error in the pressure coefficient c_p and a 1% error in the value of the extracted velocity measurement.

Keywords: Velocity measurement; Pitot tube; Low Reynolds number; Barker effect; Flat nosepiece; Hemispherical nosepiece

1. Introduction

Although the Pitot tube was invented in 1732, its usefulness as a tool for the determination of fluid velocities has been extended in recent times by the advent of electronic pressure transducers and micromanometers. In particular, such transducers have enabled the accurate reading of small pressure differences and, furthermore, have facilitated the use of automatic data acquisition systems for measurements obtained by the use of Pitot or impact tubes.

The accuracy of velocities which correspond to small pressure differences measured by means of a Pitot/impact tube was first considered by Fry and Tyndall [1]. Their work was not definitive owing to the inadequacy of the available instrumentation and to the lack of understanding of the role of the Reynolds number as a measure of the importance of viscous effects. The first definitive experiments were those performed by Barker [2]. These experiments demonstrated that the standard procedure for interpreting Pitot-tube measurements is prone to error at low Reynolds numbers.

This issue is a matter of fluid-flow fundamentals rather than the accuracy of pressure measurements themselves. The common approach to the evaluation of velocities from Pitot-tube measurements is the use of Bernoulli's equation. Among other restrictions on the use of Bernoulli's equation, one is that viscous effects are negligible. It is known, however, that external flows at low Reynolds numbers are substantially affected by viscosity [3]. Since the flow about a Pitot tube is an external flow, it is reasonable to expect that viscosity would also assert itself at Pitot-tube Reynolds numbers that are small. Consequently, the

* Corresponding author. Tel.: +1 612 625 5502; fax: +1 612 624 5230.
E-mail address: ssparr@me.umn.edu (S.K.S. Boetcher).

0017-9310/$ - see front matter © 2006 Elsevier Ltd. All rights reserved.
doi:10.1016/j.ijheatmasstransfer.2006.01.044

Nomenclature

c_p	pressure coefficient, Eq. (5)	U_∞	far-field velocity
D	outside diameter of Pitot/impact tube	u	axial component of velocity
d	diameter of aperture in Pitot/impact tube	v	radial component of velocity
L	length of truncated Pitot/impact tube	x	axial coordinate
ℓ	length of aperture	μ	viscosity
p	pressure	ρ	density
p_∞	far-field pressure		
R_{outer}	outside radius of Pitot/impact tube	*Superscript*	
Re	Reynolds number, $\rho U_\infty D/\mu$ or $\rho U_\infty R_{\mathrm{outer}}/\mu$	$'$	denotes non-dimensional variable
r	radial coordinate		

validity of the use of Bernoulli's equation for interpreting low Reynolds number, Pitot-tube data is questionable.

Barker's experiments were performed using water as the participating fluid and with the Pitot tube situated at the centerline of a round pipe. Furthermore, the Pitot tube was not equipped with static holes; that is, this type of Pitot tube is more properly characterized as a blunt-nosed *impact tube*. The static pressure was measured at the wall of the pipe. Barker's work demonstrated the inadequacy of the Bernoulli model for flows with Reynolds numbers below a threshold value. The errors in Pitot-tube velocity determinations due to the inadequacy of the Bernoulli model have been ascribed to the *Barker effect*.

Chronologically, the next experimental study of the Barker effect is that of Homann [4]. The Homann data were extended to much lower Reynolds numbers than those of Barker, thereby accentuating the Barker effect. On the other hand, in Homann's comparison of his data with those of Barker, it appears that the illustrated good agreement was due to plotting errors. In their investigation of the Barker effect, Hurd et al. [5] used an apparatus which was, in essence, a towing tank with a blunt-nosed impact tube moving through an otherwise stationary liquid. Those investigators confirmed the existence of the Barker effect but were critical of Barker's experimental technique because of alleged distortions of the velocity profile in the pipe in which the impact tube was situated. MacMillan [6] investigated the Barker effect for a blunt-nosed impact tube situated at the centerline of a developing laminar airflow in a circular tube. Macmillan compared his results with those of Barker and exposed a seeming ambiguity in the definition of Barker's Reynolds number. That ambiguity arose from a less-than-precise specification of whether Barker's indicated tube radius was either an external or internal dimension.

Another experimental study of possible relevance to the Barker effect was that of Sherman [7]. These experiments involved the use of two different geometries for the nosepieces of the investigated impact tubes. One of these is a rounded nose, termed *source-shaped* by Sherman. The other is a blunt-faced tube whose walls were tapered to a zero thickness at their most forward edge.

With regard to analysis, both Zahm [8] and Homann [9] studied the stagnation pressure at the forward edge of a solid sphere situated in uniform flow. Similarly, Lin and Schaaf [10] analyzed the stagnation point of a hemisphere. Neither of these works is actually relevant to the Barker effect because of the absence of an impact opening. An attempt was reported by Lester [11] in 1960 to apply numerical methods to the analysis of the Barker effect. The physical situation chosen for analysis was that of a blunt impact tube situated at the centerline of the fully developed laminar flow in a pipe. Since this attempt at a numerical solution was made prior to the advent of modern digital computers, it was burdened with necessary simplifying assumptions. Furthermore, the vorticity-streamfunction formulation was used, necessitating approximations in the vorticity boundary conditions. The solutions obtained by Lester were too limited to enable the identification of the threshold value at which the Bernoulli data analysis is inapplicable.

A review article dealing with the Barker effect was prepared by Chue [12]. That review does not provide any information that is not covered in the preceding paragraphs.

2. Description of the physical problem

As was described in the foregoing literature review, there is a substantial amount of experimental data which have established the existence of the Barker effect. However, as will be demonstrated later, there is so much scatter among the data that it is not possible to identify the threshold Reynolds number at which the Barker effect first asserts itself. Furthermore, as was also documented in the discussion of the literature, there appears not to have been a definitive numerical simulation of the fluid dynamics of Pitot and impact tubes. It is the objective of this work to provide such a definitive simulation and to identify quantitatively the onset of the Barker effect.

The geometries of the investigated Pitot/impact tubes are those of commonly available commercial instruments in the United States. Two types of nose geometries were investigated. One of these is a hemispherical nosepiece,

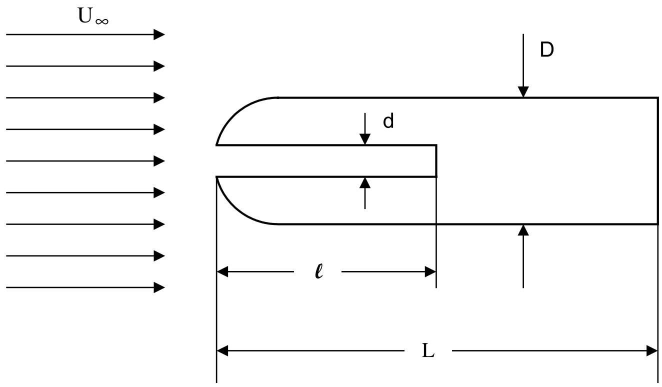

Fig. 1. Schematic of a hemispherical nosepiece attached to the body of a Pitot/impact tube.

and the second is a blunt-faced nosepiece. Both of these nosepieces had a center-hole aperture whose diameter was commensurate with those of commercial instruments. In view of the principle of geometrical similarity, it was not necessary to work with actual dimensions. Rather, only dimension ratios had to be specified.

Schematic diagrams of the Pitot/impact tubes to be studied here are presented in Figs. 1 and 2, respectively, for the hemispherical nosepiece and the blunt-faced nosepiece. As seen in Fig. 1, the simulation model encompassed only the front portion of the Pitot/impact tube. The axial length of the investigated model was demonstrated by supplementary calculations to be long enough so that the use of a greater length would not affect the flow pattern in the neighborhood of the nose. Similarly, the impact opening was truncated at a length sufficiently great so that no alteration would occur in the flow pattern if a greater length were to be used. In this regard, it may be recalled that there is no net flow into or out of the impact opening when steady-state measurements are being made. For the simulation, the ratios $L/D = 10$ and $l/d = 10$ were employed. From careful measurements of several commercially available Pitot tubes, it was found that $d/D = 0.31$ was an appropriate description of the impact aperture.

The simulation geometry for the case of the blunt-faced Pitot/impact tube is illustrated in Fig. 2. As can be seen

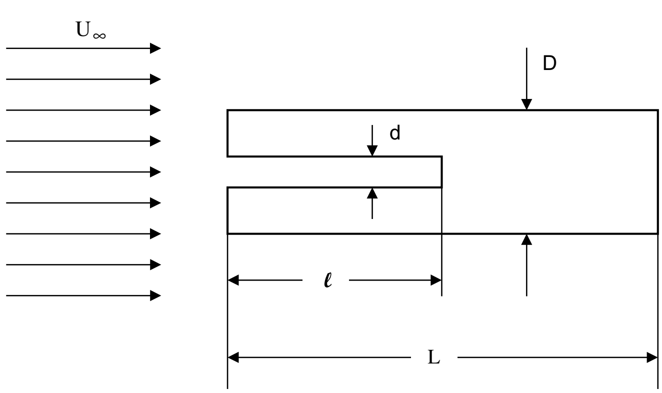

Fig. 2. Schematic of a blunt-faced nosepiece attached to the body of a Pitot/impact tube.

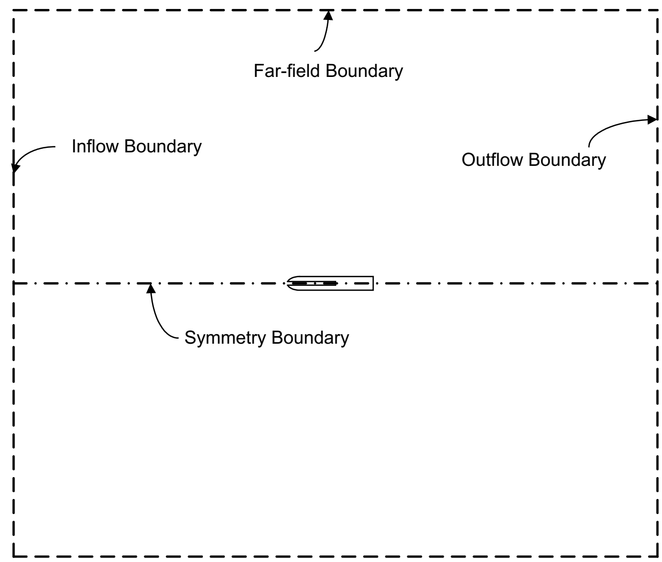

Fig. 3. The solution domain.

from a comparison of Figs. 1 and 2, the geometries of the two types of tubes are the same, except for the rounding of the nose in Fig. 1 and the squaring-off of the nose in Fig. 2.

In the numerical simulation of any external flow, the selection of the size of the solution domain is of major importance. In general, solutions are sought that are independent of the size of the solution domain. This requirement is especially important in the present situation because the viscous effects cause the fluid–solid interactions to extend forward of the nose of the Pitot/impact tube.

The solution domain that was utilized for the final computations, shown in Fig. 3, was selected on the basis of several preliminary computer runs. Each of the boundaries is labeled according to their function. At the inflow boundary, a uniform freestream velocity U_∞ was imposed, while at the symmetry boundary, all normal derivatives are zero and no flow is permitted to pass perpendicular to the boundary. At the downstream end of the solution domain, typical outflow boundary conditions are imposed. These include zero values of the streamwise first derivatives of all of the dependent variables. The upper boundary of the solution domain is treated as a *far-field* boundary. At such a boundary, the direction at which the flow crosses the boundary is unknown. The software determines the flow direction along such a boundary. The inflow boundary was positioned 20D upstream of the forward edge of the Pitot/impact tube nose, and the outflow boundary was similarly placed downstream of the trailing edge of the truncated tube. Similarly, the far-field boundary was placed at a radial distance of 20D from the centerline of the tube.

3. The governing equations

The analysis of the fluid flow was based on an axisymmetric model based on x, r cylindrical coordinates. In view of the focus of the work on very slow flows, the use of a laminar flow model was appropriate. The full Navier–Stokes equations were solved for incompressible, constant-property flow. It was found advantageous to perform the solutions in terms of dimensionless variables. To this end, let

$$u' = \frac{u}{U_\infty}, \quad v' = \frac{v}{U_\infty}, \quad p' = \frac{p}{\rho U_\infty^2}, \quad x' = \frac{x}{D}, \quad r' = \frac{r}{D}, \quad Re = \frac{\rho U_\infty D}{\mu} \tag{1}$$

Once the transformation of coordinates and variables has been made, it is convenient to drop the primes. In terms of the transformed quantities, the governing equations are

Mass conservation

$$\frac{\partial(rv)}{\partial r} + \frac{\partial(ru)}{\partial x} = 0 \tag{2}$$

Conservation of x-momentum

$$u\frac{\partial u}{\partial x} + v\frac{\partial u}{\partial r} = -\frac{\partial p}{\partial x} + \frac{1}{Re}\left(\frac{\partial^2 u}{\partial x^2} + \frac{1}{r}\frac{\partial}{\partial r}\left(r\frac{\partial u}{\partial r}\right)\right) \tag{3}$$

Conservation of r-momentum

$$u\frac{\partial v}{\partial x} + v\frac{\partial v}{\partial r} = -\frac{\partial p}{\partial r} + \frac{1}{Re}\left(\frac{\partial^2 v}{\partial x^2} + \frac{1}{r}\frac{\partial}{\partial r}\left(r\frac{\partial v}{\partial r}\right)\right) \tag{4}$$

Inspection of Eqs. (2)–(4) indicates that the only specifiable parameter is the Reynolds number based on the outer diameter of the Pitot/impact tube. It is not necessary to specify a particular fluid or to give values for any fluid properties.

Eqs. (2)–(4) were solved making use of FLUENT finite-volume-based software. The solution domain was discretized into 50,877 brick-form elements for the blunt-faced model, and 69,918 brick-form elements for the hemispherical-nosed-model. The accuracy of each solution was verified to be mesh-size independent. The actual calculations were performed using an IBM SP2 supercomputer.

The key result that was sought is the pressure difference between the upstream freestream and the stagnation point at the mouth of the Pitot/impact tube. This result is to be presented in dimensionless form as a pressure coefficient c_p defined as

$$c_p = \frac{p_{stag} - p_\infty}{\frac{1}{2}\rho U_\infty^2} \tag{5}$$

For ordinary flows, the value of c_p for the Pitot/impact tubes is 1.0 according to Bernoulli's equation. However, for slow flows, c_p may exceed 1.0 owing to the effect of viscosity. One of the goals of this research is to identify the value of the Reynolds number below which it is not correct to use $c_p = 1.0$ in interpreting Pitot/impact tube measurements.

4. Results and discussion

4.1. Threshold Reynolds number for Pitot/impact tube errors

The result of most direct practical importance is the threshold Reynolds number at which the standard Bernoulli-based interpretation of Pitot/impact tube data ceases to be applicable. The deviations from the Bernoulli-based model are presented in Fig. 4. In that figure, the pressure coefficient c_p, defined by Eq. (5), is plotted as a function

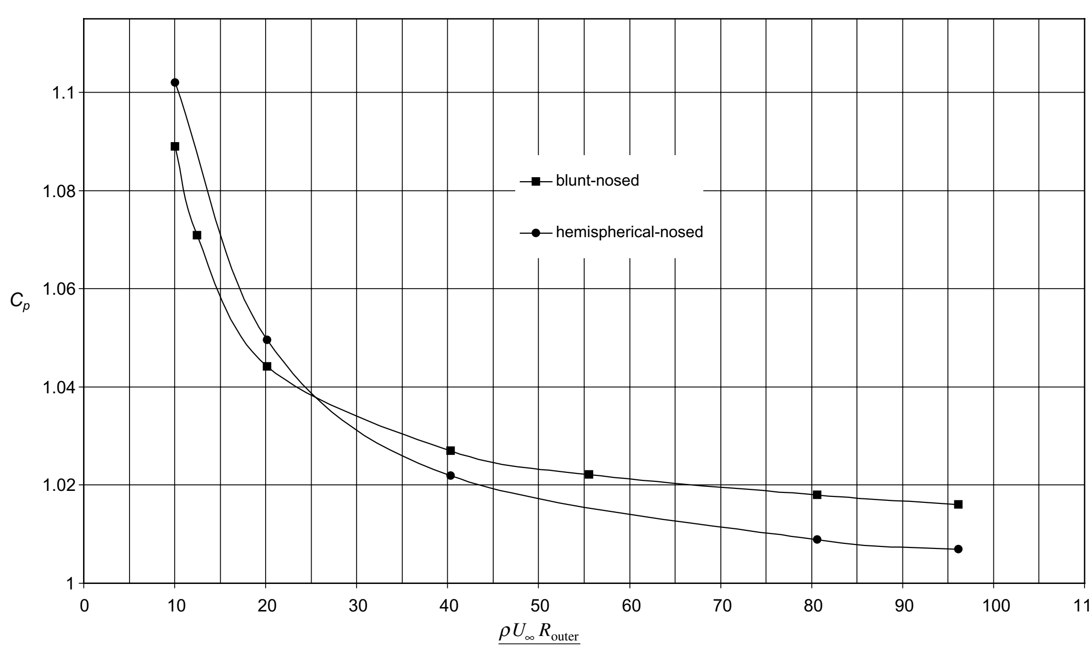

Fig. 4. Low Reynolds number deviations from the Bernoulli-based Pitot/impact tube model $c_p = 1$.

of the Reynolds number of the Pitot/impact tube. Special note should be taken of the definition of the Reynolds number which appears on the abscissa of the figure. That Reynolds number is based on the *outside radius* R_{outer} of the tube. This practice is used here because it is the traditional way for presenting Pitot/impact tube data.

Observation of Fig. 4 indicates that for the Reynolds range investigated, $c_p > 1$. In general, the lower the Reynolds number, the higher the value of c_p. On the other hand, c_p approaches 1 at sufficiently high values of the Reynolds number. For practical purposes, it is reasonable to define the threshold of deviations from the standard Bernoulli interpretation in terms of an acceptable level of accuracy in the velocity determination. The writers have selected the threshold as corresponding to

$$c_p = 1.02 \tag{6}$$

This 2% deviation of c_p from unity corresponds to an error of 1% in the velocity determination. For practical purposes, this is believed to be a viable definition of the onset of non-Bernoulli effects.

Further inspection of the figure reveals the following threshold Reynolds numbers for the two types of Pitot/impact tube geometries:

$$Re_{\mathrm{threshold}} \cong 65 \text{ for the blunt-faced tube} \tag{7}$$

$$Re_{\mathrm{threshold}} \cong 45 \text{ for the hemispherical-nosed tube} \tag{8}$$

At a Reynolds number of approximately 10, the value of c_p is about 1.1, which corresponds to an error of 5% if the Bernoulli model were used in the determination of the velocity.

4.2. Collection of all available information relating to the Barker effect

It is relevant to bring together all of the prior information, both experimental and analytical-numerical, to place the present results in the context of the history of the Barker effect. To this end, Fig. 5 has been prepared. The figure displays six sets of experimental data as well as five analytical and numerical contributions. As was noted in the introduction, Barker's data constitute the first serious attempt at quantifying the domain in which the standard Bernoulli-based interpretation of Pitot/impact tube data fails. As can be seen from Fig. 5, there is considerable scatter among the Barker data, in all likelihood due to the insufficiency of the instrumentation. The second experimental contribution, that due to Homann, presents a dilemma. In Homann's paper, his data seem to fall among a scatter-free rendering of Barker's data. On the other hand, that rendering appears to be a misrepresentation of the actual Barker data. Furthermore, Homann indicates that both his data and Barker's data lie along an analytical characterization of the pressure coefficient for a sphere without an aperture [8]. That characterization is, however, clearly incorrect as will be demonstrated shortly.

The data of Hurd, et al., Sherman, and MacMillan were reported at virtually the same time. Hurd's and Sherman's (flat-nosed) data are qualitatively reinforcing, while MacMillan displays the minimum viscous effects among all of the information exhibited in Fig. 5. The results of the present numerical simulation appear to fit satisfactorily with both Hurd's and Sherman's (flat-nosed) data.

With regard to the analytical and numerical results, those of Lin and Schaaf, Homann, and Zahm are not really

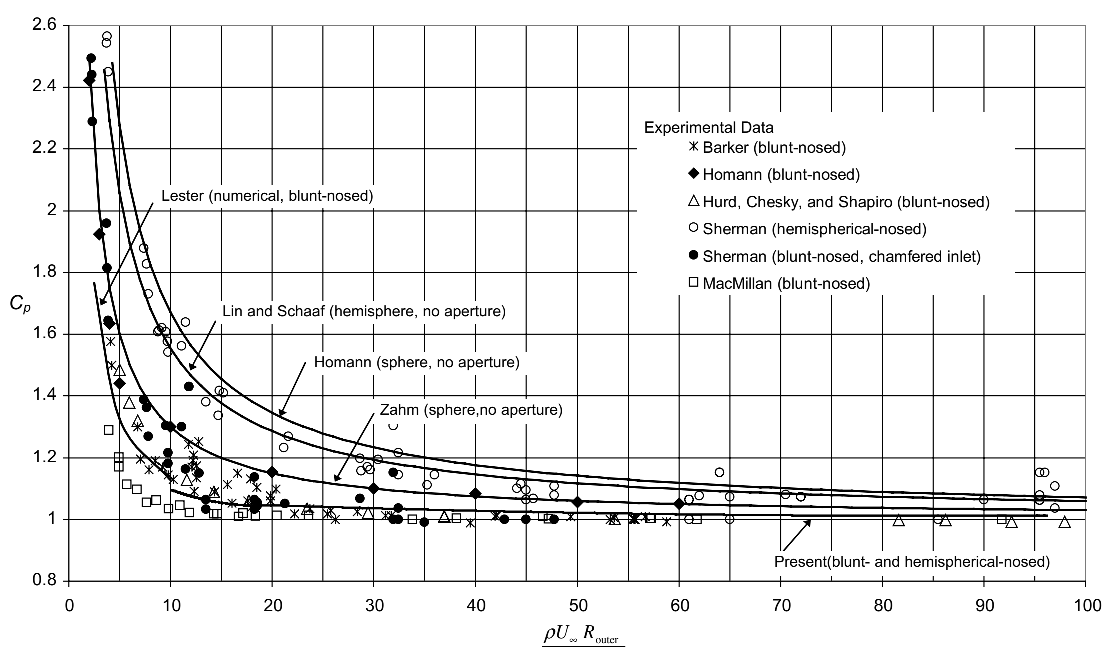

Fig. 5. Compilation for all available information for the Barker effect.

appropriate to the Pitot/impact tube situation in that they did not consider any impact opening aperture. Furthermore, a comparison of the Homann and Zahm results, both purported to apply to a sphere, shows considerable disagreement. It is the view of the present authors that Zahm's result is in error. The only other numerical work that has heretofore been available is that of Lester. It is remarkable that despite the absence of computational resources and the concomitant need for simplifying assumptions, Lester's results appear to be a reasonable extension of those obtained here.

4.3. Streamline patterns adjacent to the nose of the Pitot/impact tube

To provide further understanding of the causes of the Barker effect, it is relevant to examine the streamline pattern adjacent to the nose of the Pitot/impact tubes that were studied here. In addition to the two nose geometries, the variation of the streamline pattern with the Reynolds number is also relevant.

Fig. 6 has been prepared to illustrate the streamline patterns for the case of the blunt-faced nose. Part (a) of the figure corresponds to $\rho U_\infty R_{\text{outer}}/\mu = 10$, while part (b) is for $\rho U_\infty R_{\text{outer}}/\mu = 96$. The pictured streamlines correspond to dimensionless values that are identical for the two figures. Inspection of Fig. 6(a) reveals that the nose-adjacent streamline begins to turn earlier to escape the blockage due to the tube's presence than does the corresponding streamline in Fig. 6(b). This observation indicates that the precursive effect due to viscosity extends farther upstream for the lower Reynolds number flow than for the higher Reynolds number flow.

A similar exposition is presented in Fig. 7 for the case of the hemispherical-nosed Pitot/impact tube. Once again, parts (a) and (b) correspond, respectively, to Reynolds numbers of 10 and 96. These figures display a streamline pattern that is generally similar to those of Fig. 6 for the case of the flat-nosed tube. For the lower Reynolds number, Fig. 7(a), the nose-adjacent streamline begins to turn away from its straight path at a greater distance from the nose than for the case of the higher Reynolds number, Fig. 7(b).

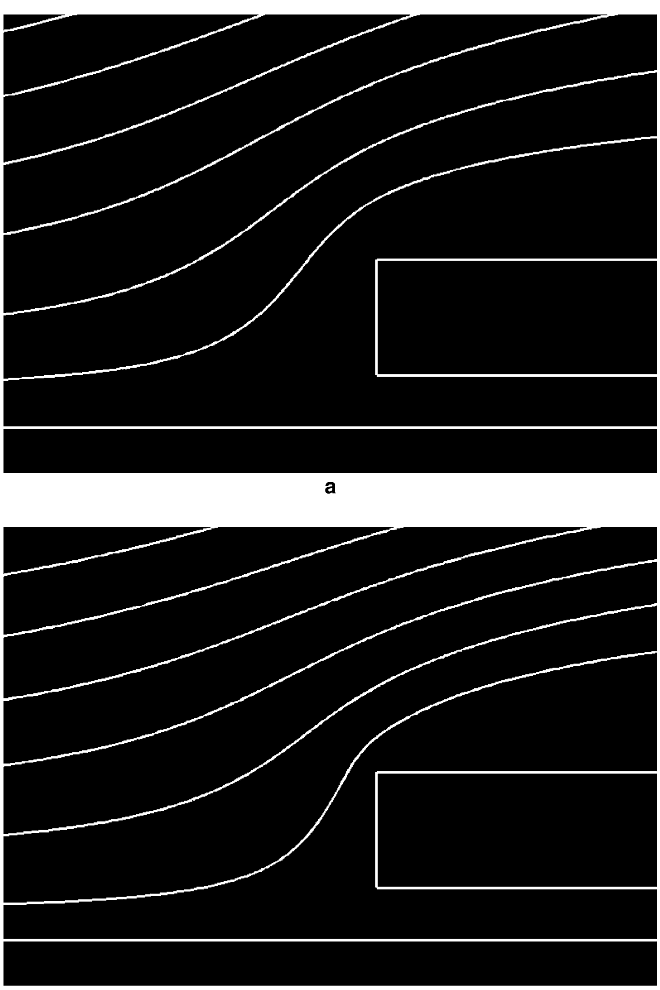

Fig. 6. Streamline patterns adjacent to a blunt-faced nose: (a) $\rho U_\infty R_{\text{outer}}/\mu = 10$ and (b) $\rho U_\infty R_{\text{outer}}/\mu = 96$.

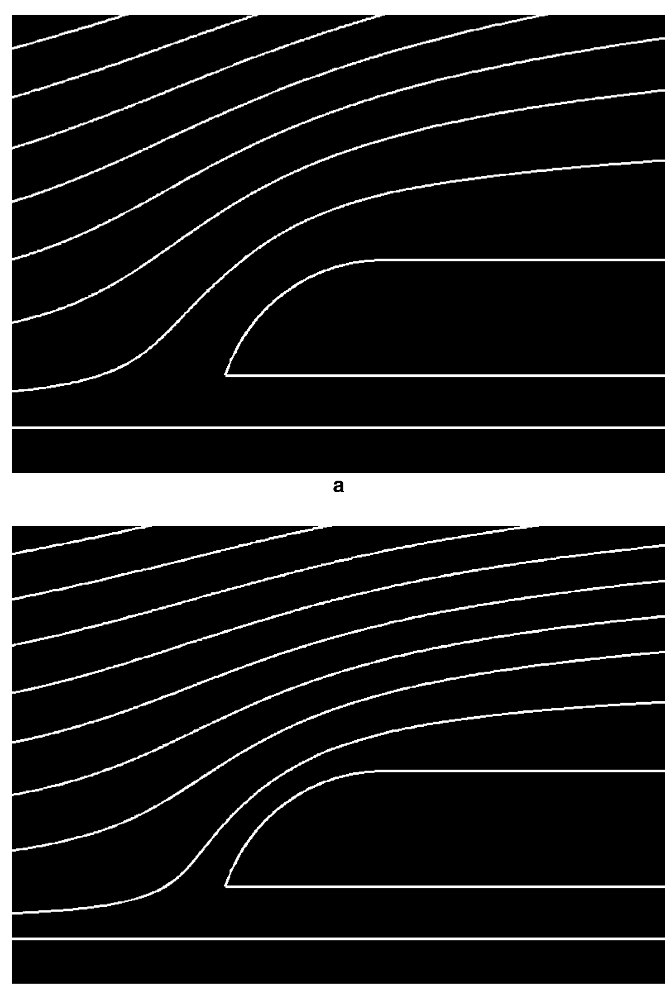

Fig. 7. Streamline patterns adjacent to a hemispherical nose: (a) $\rho U_\infty R_{\text{outer}}/\mu = 10$ and (b) $\rho U_\infty R_{\text{outer}}/\mu = 96$.

Figs. 6 and 7 display only a portion of the flow field that was provided by the numerical simulations. A careful examination of the entire flow field (not shown here) clearly indicates that the size of the solution domain was properly chosen sufficiently large to assure results of high accuracy.

5. Concluding remarks

This investigation was undertaken to provide a definitive conclusion to an important problem in fluid flow measurement which has been characterized by a considerable degree of disorder (Fig. 5) in the past. The data identifying the viscous-related errors in the measurement of low fluid velocities by Pitot/impact tubes were collected in six individual experimental investigations, the first being that of Barker in 1922. The viscous-driven presence of a precursive extension of the flow field upstream of the nose of the tube serves to invalidate the standard Bernoulli equation interpretation of Pitot/impact tube data. The threshold at which the Bernoulli interpretation first fails has not been established in any reliable manner in the past, especially because of considerable scatter in the experimental data.

The analytical contributions to the subject have been primarily for nosepieces that do not have an impact aperture. The absence of such an aperture means that the results for these models do not apply directly to Pitot/impact tubes. The one attempt at numerical simulation of the problem was carried out at a time when the available computational assets were minimal, so that it was necessary to make a considerable number of simplifying assumptions to implement the numerical work.

As a consequence, a definitive criterion for the breakdown of the Bernoulli interpretation has been absent. Such a criterion has been obtained here from detailed numerical simulations of the flow about Pitot/impact tubes equipped with either one of two types of nosepieces. One of these is a blunt-faced nose while the other is a hemispherical nose. The model that was implemented provided freedom for the flow arriving at the impact opening to follow its own path without constraint.

It is found that the criterion for the breakdown of the Bernoulli interpretation occurred at a value of $\rho U_\infty R_{\text{outer}}/\mu = 45$ for the hemispherical-nosed tube and at $\rho U_\infty R_{\text{outer}}/\mu = 65$ for the blunt-nosed tube. These criteria correspond to a deviation of the pressure coefficient c_p of 2% from the standard Bernoulli result. This 2% deviation of the pressure coefficient corresponds to a 1% deviation in the velocity itself. The calculations for both types of tubes were extended to values of $\rho U_\infty R_{\text{outer}}/\mu = 10$, at which point the pressure coefficient is approximately 1.1.

The streamline patterns adjacent to the nose of each of the investigated tubes reveal the extent of the precursive effect due to viscosity. The lower the Reynolds number, the farther upstream did the precursive effect extend.

Acknowledgement

Computational resources are provided by the Minnesota Supercomputing Institute for Digital Simulation and Advanced Computation.

References

[1] J.D. Fry, A.M. Tyndall, On the value of the Pitot constant, Philos. Mag. Ser. 6 (21) (1911) 348–366.
[2] M. Barker, On the use of very small Pitot-tubes for measuring wind velocities, Proc. Roy. Soc. A 101 (1922) 435–445.
[3] H. Schlichting, Boundary-layer Theory, seventh ed., McGraw-Hill Book Company, New York, 1979.
[4] F. Homann, Einfluß großer Zähigkeit bei Stömung um Zylinder, Forschung auf dem Gebiete des Ingenieurwesens, 1936, pp. 1–10.
[5] C.W. Hurd, K.P. Chesky, A.H. Shapiro, Influence of viscous effects on impact tubes, J. Appl. Mech. (1953) 253–256.
[6] F.A. MacMillan, Viscous effects on Pitot tubes at low speeds, J. Roy. Aeronaut. Soc. 58 (1954) 570–572.
[7] F.S. Sherman, New experiments on impact pressure interpretation in supersonic and subsonic rarefied airstreams, NACA TN 2995, 1953.
[8] A.F. Zahm, Pressure of air on coming to rest from various speeds, NACA TR 247, 1926.
[9] F. Homann, The effect of high viscosity on the flow around a cylinder and a sphere, NACA TM 1334, 1952.
[10] T.C. Lin, S.A. Schaaf, The effect of slip on flow near a stagnation-point and in a boundary layer, NACA TN 2568, 1951.
[11] W.G.S. Lester, The flow past a Pitot tube at low Reynolds numbers, Brit. ARC R&M 3240, 1961.
[12] S. Chue, Pressure probes for fluid measurement, Prog. Aerospace Sci. 16 (2) (1975) 147–223.